International Journal of Minerals, Metallurgy and Materials
Volume 28, Number 1, January 2021, Page 66
https://doi.org/10.1007/s12613-020-2036-x

Behavior of phosphorus enrichment in dephosphorization slag at low temperature and low basicity

Ge-fan Ye, Jian Yang, Run-hao Zhang, Wen-kui Yang, and Han Sun

State Key Laboratory of Advanced Special Steel, School of Materials Science and Engineering, Shanghai University, Shanghai 200444, China
(Received: 7 January 2020; revised: 4 March 2020; accepted: 6 March 2020)

Abstract: At low basicity and low temperature, the dephosphorization behavior and phosphorus distribution ratio (L_P) between slag and molten steel in the double slag and remaining slag process were studied with a 180 t basic oxygen furnace industrial experiment. The dephosphorization slags with different basicities were quantitatively analyzed. At the lower basicity range of 0.9–2.59, both L_P and dephosphorization ratio were increased as the basicity of dephosphorization slag increased. Dephosphorization slag consisted of dark gray P-rich, light gray liquid slag, and white Fe-rich phases. With increasing basicity, not only did the morphologies of different phases in the dephosphorization slag change greatly, but the area fractions and P_2O_5 content of the P-rich phase also increased. The transfer route of P during dephosphorization can be deduced as hot metal → liquid slag phase + Fe-rich phase → P-rich phase.

Keywords: dephosphorization; basicity; phosphorus-rich phase; slag; converter steelmaking

1. Introduction

Multi-refining converter (MURC) process [1], which was developed by Nippon Steel, is the dephosphorization process in basic oxygen furnace (BOF) that can markedly decrease calcium oxide (CaO) consumption and waste slag emission. Desilication and dephosphorization are first conducted. After intermediate deslagging by tilting the furnace, decarburization is further performed in the same converter. Then, the decarburization slag is left after tapping and reused for the dephosphorization in the next heat because of the lower temperature at the early stage of converter blowing, which is favorable to dephosphorization. Therefore, consumption of lime and light-burned dolomite can be greatly reduced along with the emission amount of waste slag. According to the report [2], the lime consumption is reduced by 40% compared with the conventional BOF process during the entire converter blowing. To steadily enhance the deslagging ratio of the MURC process by more than 70%, we have to adjust the slag composition and top-blowing lance position to control the slag-foaming condition [3].

Regarding the effects of dephosphorization operation parameters in the double slag and remaining slag process similar to MURC, Wang *et al.* [4] found that the fluidity of the dephosphorization slag can be improved at lower basicity (R of 1.3–1.5), and the slag has a moderately foaming property, thereby enhancing the deslagging ratio after dephosphorization. Yang *et al.* [5] studied the effect of operation factors on dephosphorization performance under the lower initial phosphorus content less than 0.09wt% of hot metal; they reported that dephosphorization is determined by the mass transfer of phosphorus from metal/slag interface to bulk slag phase rather than the thermodynamic equilibrium conditions. Tian *et al.* [6] showed that the dephosphorization ratio can reach 75% in the dephosphorization stage, when the Fe^{3+} content in the slag is higher than 3.5wt%, the basicity is higher than 2.0, and the temperature is lower than 1653 K. Lü *et al.* [7] found that the viscosity of CaO–SiO_2–"FeO"–12wt%ZnO–3wt%Al_2O_3 slags decreases as the CaO/SiO_2 mass ratio increases from 0.8 to 1.2 and the FeO content also increases from 8wt% to 20wt%.

In the dephosphorization process, $2CaO{\cdot}SiO_2$–$3CaO{\cdot}P_2O_5$ (C_2S–C_3P) in the dephosphorization slag plays an important role [8]. In the hot metal dephosphorization reaction, the slag is in a solid/liquid multiphase coexistence state. However, in most previous studies, the slag was taken as a liquid phase while the solid phase was ignored. The partition ratio of phosphorus between C_2S–C_3P and the liquid slag was usually extremely high during the dephosphorization stage because phosphorus was more stable in the solid solution

Corresponding author: Jian Yang E-mail: yang_jian@t.shu.edu.cn

C_2S–C_3P than in the liquid slag [9]. Dicalcium silicate C_2S is precipitated initially, and then the P_2O_5 component is reacted with CaO to form tricalcium phosphate C_3P. Subsequently, the formed C_3P is combined with the produced C_2S to generate solid solution C_2S–C_3P [10–12]. Gao *et al.* [13–14] pointed out that the solid phase coexisting with the liquid slag is the solid solution composed of CaO, SiO_2, and P_2O_5, and phosphorus is distributed mainly in the solid solution rather than in the liquid phase. The solid solution only exists as C_2S–C_3P, and the mass ratio between the solid solution and liquid slag phases varies with the liquid-phase composition in the slag.

The transfer of phosphorus from liquid slag to the solid solution of C_2S–C_3P has a significant influence on dephosphorization. Kitamura *et al.* [15] found that the mass transfer of CaO and SiO_2 can occur simultaneously with the mass transfer of P_2O_5 to maintain the pseudo-binary relation of the solid solution. Xie *et al.* [16] discovered that the transfer rate of phosphorus from the liquid slag to the solid solution of C_2S–C_3P is very high. Inoue and Suito [17] indicated the minimal temperature dependence of phosphorous distribution ratio between C_2S and slag. Shimauchi *et al.* [18] showed that the content of P_2O_5 in the solid solution is strongly influenced by the lime/silica mass ratio and P_2O_5 content in the liquid slag. Yang *et al.* [19–21] found that the higher temperature induces the dissolution of the C_2S–C_3P solid solution while the larger CaO/SiO_2 mass ratio has the opposite effect. Du *et al.* [22] discovered that the distribution ratio of P_2O_5 between the solid solution and liquid phase slag is increased as the Fe_2O_3 content and slag basicity increase. Lin *et al.* [23] revealed that the contents of CaO, T.Fe (total Fe content), and P_2O_5 in slag significantly affect the distribution of P_2O_5 between the P-rich and liquid slag phases, whereas the contents of MnO and MgO have a minimal effect. Pahlevani *et al.* [24] indicated that the CaO content of the liquid slag and the activity of P_2O_5 in the solid solution are the ruling factors for the distribution ratio of phosphorus between the solid solution and the liquid slag.

Regarding the effect of the Fe-rich phase in the slag on dephosphorization, Ito and Terasawa [25] found that the CaO–FeO layer is formed when the solid CaO is reacted with the P_2O_5-containing slag at the hot metal temperature. Hamano *et al.* [26] observed that Fe^{2+} diffuses to both the solid CaO and bulk slag, and the CaO–FeO layer is formed beside the solid CaO because of the activity gradient of FeO. The CaO–FeO phase can promote the generation of the solid solution C_2S–C_3P and increase the phosphorus partition ratio between the C_2S–C_3P and liquid slag phase [27]. Xie and Wang [28] found that the phase ratio of the C_2S–C_3P solid solution increases as the FeO_t and P_2O_5 contents increase.

As stated above, relatively few industrial experiments have been conducted on the effect of the basicity of slag on dephosphorization at the lower basicity of 0.9–2.59 and at the lower temperature of 1646–1693 K, which correspond to favorable dephosphorization conditions in the double slag and remaining slag process. Few studies have conducted quantitative analysis of the P-rich and Fe-rich phases and their relationship based on industrial experiments. Therefore, in-depth studies are needed to clarify the effect of basicity on the dephosphorization and slag phases at the lower basicity and temperature ranges, especially based on the industrial experiments.

In this study, at a lower basicity range, the effects of basicity on the dephosphorization ratio and phosphorus distribution ratio (L_P) between slag and molten steel were studied at the dephosphorization stage in the double slag and remaining slag process through industrial experiments with a 180 t converter. The morphologies of low basicity dephosphorization slag were observed. The P-rich and Fe-rich phases and their relationship were quantitatively analyzed through field emission scanning electron microscopy (FESEM) coupled with energy dispersive spectroscopy (EDS). The element compositions of the different slag phases were also analyzed to study the behavior of phosphorus enrichment in the dephosphorization slag.

2. Experiment and principle

2.1. Experimental procedure

Experiments were conducted in the 180 t converter for the double slag and remaining slag process. Fig. 1 shows the schematic flowsheet of the double slag and remaining slag process. Desiliconization and dephosphorization were conducted initially. After intermediate deslagging, decarburiza-

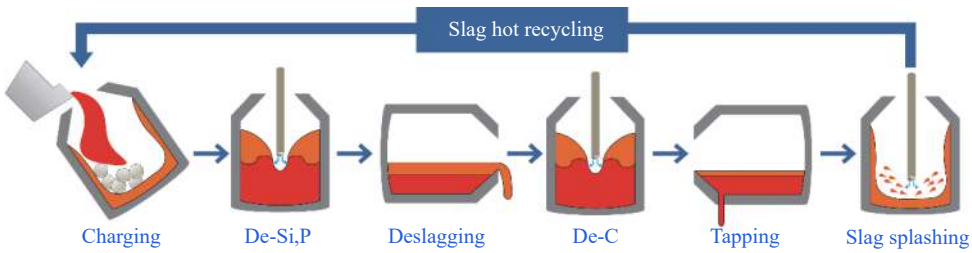

Fig. 1. Schematic flowsheet of double slag and remaining slag process (De-Si,P—Desiliconization and dephosphorization; De-C—Decarburization).

tion was conducted in the same converter. Then, the decarburization slag was left inside the furnace after tapping and slag splashing, and reused for dephosphorization in the next heat.

As the temperature is low in the early stage of converter blowing and favorable for dephosphorization from a thermodynamic point of view, dephosphorization reaction can be conducted at low basicity. On the one hand, it can greatly reduce the consumption of lime. On the other hand, it is conducive to the formation of the slag with good fluidity to improve the ratio of intermediate deslagging. At the end of converter blowing, because the high temperature is not conducive to dephosphorization, dephosphorization reaction can only occur at high basicity, which increases the consumption of lime. Therefore, adopting low temperature and low basicity in the early dephosphorization stage is necessary in the double slag and remaining slag process.

The process flow of the double slag and remaining slag process is similar to that of MURC. However, the bottom-blowing intensity of the double slag and remaining slag process is usually weaker than that of MURC. The supply intensity of the bottom gas of MURC was 0.4–0.8 $Nm^3/(t·min)$ [1], whereas that of the double-slag process and remaining slag process was 0.02–0.15 $Nm^3/(t·min)$. In addition, the slag splashing technology was applied after tapping in the double slag and remaining slag process.

The composition and temperature (T) of hot metal for dephosphorization are shown in Table 1. The hot metal after desulfurization was charged into BOF with temperature of 1573–1673 K. The initial P content in hot metal had a relatively high value of 0.13wt%–0.18wt%, and the mass ratio between the hot metal and the total added iron was in the range of 84%–88%. Among the other auxiliary raw materials were lime, magnesite, raw dolomite, limestone, and sinter, which were charged into BOF by two batches in the dephosphorization and decarbonization stages, respectively. The top oxygen-blowing time at the dephosphorization stage was 4–6 min. The gas supply intensity of the top oxygen blowing was 2.2–3.0 $Nm^3/(t·min)$. The height of the lance position was changed during the dephosphorization stage, and the initial low lance position was 1.8 m, which could promote the ignition of top oxygen blowing. Then, the high lance position was 2.0 m to enhance the oxidization of the slag and promote the rapid melting of lime and the other auxiliary raw materials. The later low lance position was 1.8 m for favoring dephosphorization reaction.

Table 1. Composition and temperature of hot metal for dephosphorization

Composition / wt%					Temperature / K
C	Si	Mn	P	S	
4.3–4.7	0.20–0.50	0.10–0.20	0.13–0.18	0.004–0.008	1573–1673

2.2. Thermodynamic principle of dephosphorization

According to the molecular structure theory of slag, dephosphorization is a slag–metal interface reaction, and the reaction equation is expressed as follows:

$$2[P] + 5(FeO) + 3(CaO) = (3CaO·P_2O_5) + 5[Fe] \quad (1)$$

The reaction equilibrium constant ($K^{\ominus}$) of dephosphorization can be expressed as follows:

$$\lg K^{\ominus} = \lg \frac{a_{(3CaO·P_2O_5)}}{[\%P]^2 a^5_{(FeO)} a^3_{(CaO)}} \quad (2)$$

where $a_{(3CaO·P_2O_5)}$, $a_{(FeO)}$, $a_{(CaO)}$ are the activities of $3CaO·P_2O_5$, FeO, and CaO, respectively; [%P] is the mass percentage of phosphorus in the molten steel.

Due to the very low content of $3CaO·P_2O_5$ in the slag, the mole fraction of P_2O_5 ($x_{(P_2O_5)}$) is equal to that of $3CaO·P_2O_5$ ($x_{(3CaO·P_2O_5)}$), namely, $x_{(3CaO·P_2O_5)} = x_{(P_2O_5)}$. Therefore, the theoretical phosphorus distribution ratio (L^1_P) between slag and molten steel is calculated according to the following equation:

$$\lg L^1_P = \lg \frac{x_{(P_2O_5)}}{[\%P]^2} = \lg(K^{\ominus} a^5_{(FeO)} a^3_{(CaO)}) \quad (3)$$

Considering the formula of L^1_P, we can conclude that the affecting factors are temperature, basicity, and the activity of FeO in the slag. In the present study, the effects of the slag basicity on dephosphorization are mainly investigated at the dephosphorization stage in the double slag and remaining slag process.

The dephosphorization slag was sampled after the dephosphorization reaction. The samples were prepared by grinding with SiC paper up to 1200 grit followed by polishing using 0.03 μm diamond powder. After surface carbonization, the samples were observed by FESEM (Nova Nano SEM450, FEI, Czech Republic) equipped with an energy dispersive spectrometer (X-MaxN, Oxford Instruments, United Kingdom), which is operated in backscattered electron (BSE) imaging mode for morphology and composition analyses. Optical microscope (OM, DM2700 M, Leica, Germany) was used for the petrographic analysis, and X-ray diffraction (XRD, D8 Advance, Bruker AXS, Germany) was used for the phase analysis of dephosphorization slag.

3. Results and discussion

3.1. Results of dephosphorization period

At the end of the dephosphorization stage, the top oxygen blowing was stopped. After intermediate deslagging by tilting the furnace for approximately 1–5 min, the molten steel

and slag were sampled for component analysis. Tables 2 and 3 are the compositions of molten steel and dephosphorization slag after the dephosphorization reaction in double slag and remaining slag process, respectively. The composition of molten steel was analyzed by the direct-reading spectrometer, and the composition of dephosphorization slag was analyzed by X-ray fluorescence. The contents of P_2O_5 in the slag are higher than 4wt% at the basicity greater than 1.90. R is the value of binary basicity of CaO/SiO_2, and De-P ratio is the dephosphorization ratio. The slag basicity at the end of dephosphorization stage varied from 0.9 to 2.59, which was controlled by adding the different amounts of lime.

Table 2. Compositions, temperatures (T), and dephosphorization ratios of molten steels after dephosphorization at different basicities

R	Composition of molten steel / wt%					T / K	De-P ratio
	C	Si	Mn	P	S		
0.90	2.6082	0.009	0.099	0.1413	0.0180	1683	10
1.28	2.8743	0.012	0.078	0.1225	0.0247	1693	19
1.68	2.6851	0.027	0.0094	0.0998	0.0098	1651	32
1.90	2.7119	0.001	0.124	0.0854	0.0277	1646	49
2.20	2.6712	0.026	0.148	0.0682	0.0203	1692	52
2.59	2.5568	0.009	0.101	0.0586	0.0113	1653	55

Table 3. Compositions of dephosphorization slags after the dephosphorization reaction at different basicities

R	Dephosphorization slag composition / wt%						
	Al_2O_3	CaO	MgO	MnO	P_2O_5	SiO_2	T.Fe
0.90	1.64	25.94	7.32	11.79	1.33	28.69	16.85
1.28	1.35	33.22	9.10	8.38	2.80	26.05	14.35
1.68	1.27	33.84	6.40	8.48	3.19	20.12	16.25
1.90	3.10	36.31	7.33	9.27	4.92	19.12	15.33
2.20	1.92	38.26	8.84	5.45	4.37	17.40	14.93
2.59	1.25	38.85	7.82	6.79	4.91	14.98	18.36

3.2. Effect of basicity of dephosphorization slag on phosphorus distribution ratio and dephosphorization ratio

The calculation of theoretical phosphorus distribution ratio L_P^1 is difficult because dephosphorization reaction in the converter is a non-equilibrium reaction and the influences of the slag structures and compositions on dephosphorization are complex. According to the previous research results, the empirical equations for calculating L_P are summarized in Table 4.

In Table 4, (%T.Fe), (%CaO), (%MgO), (%MnO), ($\%P_2O_5$), ($\%SiO_2$), and (%FeO) are the contents of T.Fe, CaO, MgO, MnO, P_2O_5, SiO_2, and FeO in the slag, respectively; T is the temperature of the molten steel in K; [%C] is the carbon content in the molten steel.

Table 4. Empirical equations for calculating L_P value

Empirical equation		Ref.
$\begin{cases} \lg L_P = 22350/T - 23.7 + 7\lg(\%CaO) + 2.5\lg(\%T.Fe) & ((\%CaO) \geq 30wt\%) \\ \lg L_P = 22350/T - 16 + 0.08(\%CaO) + 2.5\lg(\%T.Fe) & ((\%CaO) < 30wt\%) \end{cases}$	(4)	[29]
$\lg L_P = 0.072((\%CaO) + 0.3(\%MgO) + 0.6(\%P_2O_5) + 0.6(\%MnO)) + 2.5\lg(\%T.Fe) + 11570/T - 10.52$	(5)	[30]
$\lg L_P = 2.5\lg(\%T.Fe) + 0.0715((\%CaO) + 0.25(\%MgO)) + 7710/T - 8.55 + (105.1/T + 0.0723)[\%C]$	(6)	[1]
$\lg L_P = 0.072((\%CaO) + 0.15(\%MgO) + 0.6(\%P_2O_5) + 0.6(\%MnO)) + 2.5\lg(\%T.Fe) + 11570/T - 10.52$	(7)	[31]
$\lg L_P = (1/T)\cdot(162(\%CaO) + 127.5(\%MgO) + 28.5(\%MnO)) + 2.5\lg(\%FeO) + 11000/T - 6.28 \times 10^{-4}(\%SiO_2) - 10.4$	(8)	[32]

Fig. 2 shows the comparison of L_P at the different basicities of dephosphorization slag between the experimental and calculated values with the different empirical formulas. The experimental values of L_P are calculated by the formula of $\lg L_P = \lg((\%P)/[\%P])$ according to the data shown in Tables 2 and 3, where (%P) and [%P] are the phosphorus contents in the dephosphorization slag and molten steel, respectively. The other values of L_P are calculated with the different empirical equations listed in Table 4.

As shown in Fig. 2, L_P has an upward trend with the increasing basicity of the dephosphorization slag. Moreover, the experimental values of L_P are much smaller than those calculated by different empirical equations. The experimental values of L_P are relatively close to those calculated by Eq. (6) because most of these formulas are the results at the endpoint of converter decarburization, which has higher basicity

and temperature. Only Eq. (6) focuses on the results of the lower basicity and temperature for the dephosphorization stage in the double slag and remaining slag process. Moreover, this formula considers the influence of C content in the molten steel on L_P, which is suitable for the higher carbon content in the dephosphorization stage of this process. On the other hand, the experimental values of L_P in this study are the results under non-equilibrium conditions. The dephosphorization times in the dephosphorization period of this process are only 4–6 min, and the dephosphorization reaction is far from reaching equilibrium. Therefore, the calculated L_P values of Eq. (6) are higher than those of the experimental ones.

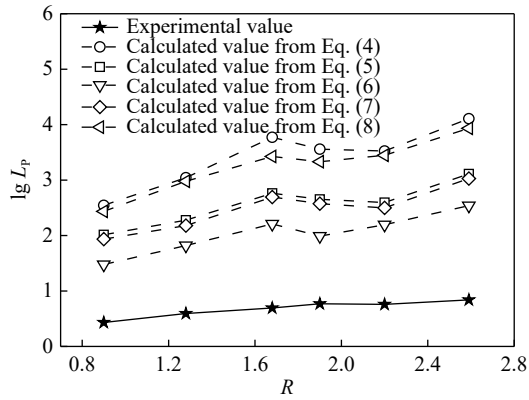

Fig. 2. Comparison of L_P at different basicities of dephosphorization slag between experimental and calculated values with different empirical equations in Table 4.

Fig. 3 illustrates the effects of the basicity of dephosphorization slag on P content in molten steel and De-P ratio at the end of the dephosphorization stage. With increasing R, P content in molten steel decreases, whereas the De-P ratio increases. In the process of converter blowing, P in the molten steel is oxidized to form P_2O_5 and then combined with CaO in the slag to form C_3P to become stable in slag. Increasing the basicity can reduce the activity of P_2O_5, which is beneficial to

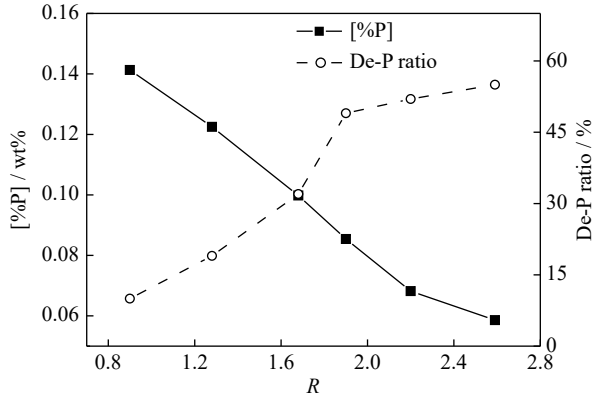

Fig. 3. Effect of basicity of dephosphorization slag on P content in molten steel ([%P]) and De-P ratio at the endpoint of dephosphorization.

the dephosphorization reaction. As L_P increases with increasing basicity, increasing the basicity of dephosphorization slag enhances the De-P ratio.

3.3. Phase analysis of dephosphorization slag

Fig. 4 shows a petrographic image of the dephosphorization slag with the basicity of 2.59 by OM. The dephosphorization slag is divided into three phases, including dark gray phase 1, light gray phase 2, and white phase 3, and the boundaries of these phases are very clear.

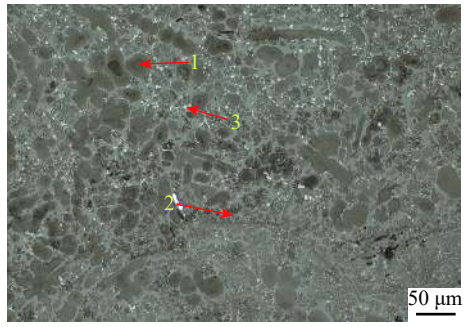

Fig. 4. Petrographic image of dephosphorization slag with the basicity of 2.59.

Fig. 5 shows the XRD analysis result of dephosphorization slag with the basicity of 2.59. Fig. 6 shows the FESEM images of the same dephosphorization slag under the different magnifications, which vary from 500 to 20000. As shown in Fig. 5, the dephosphorization slag consisted of solid solution (C_2S–C_3P), the silicate phase ($Ca_3Mg(SiO_4)_2$), and the calcium ferrite phase ($Ca_2Fe_2O_5$). According to the FESEM images in Fig. 6, the dephosphorization slag consisted of three phases: dark gray phase 1, light gray phase 2, and white phase 3 at magnification of 10000. The dark gray phase 1 and white phase 3 are dispersed, while the light gray phase 2 has a relatively continuous distribution.

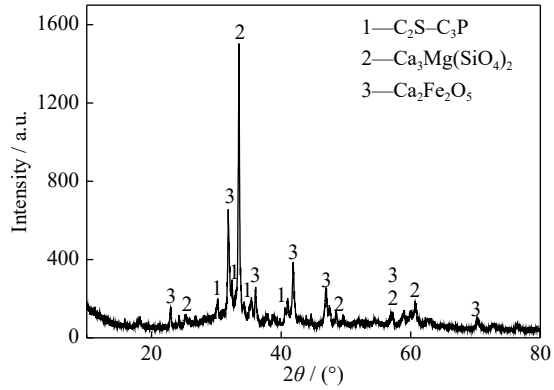

Fig. 5. XRD analysis result of dephosphorization slag with the basicity of 2.59.

In the dephosphorization period of converter blowing, dephosphorization slag is in a state of solid–liquid phase coex-

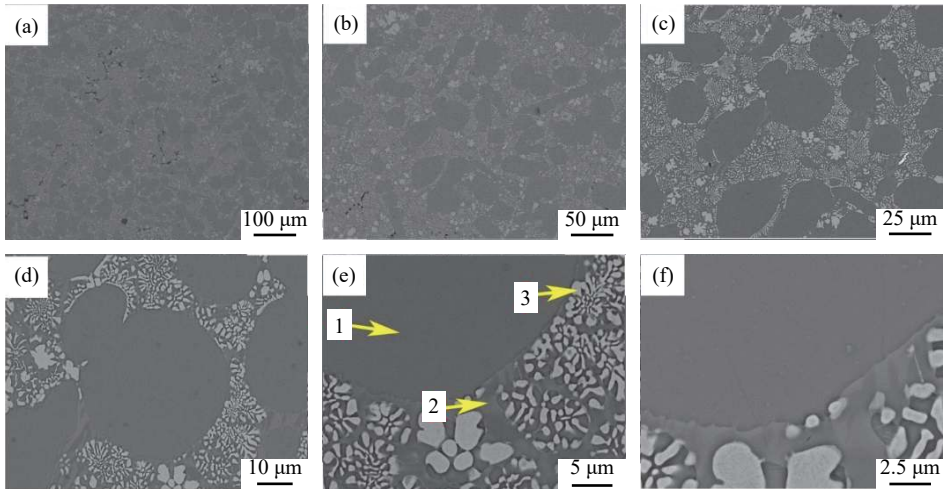

Fig. 6. FESEM images of dephosphorization slag with the basicity of 2.59 under different magnifications: (a) 500; (b) 1000; (c) 2000; (d) 5000; (e) 10000; (f) 20000.

istence. During the process of converter blowing, after the lime is melted, CaO, SiO_2, and P_2O_5 in the liquid slag react to form C_2S and C_3P, and then the solid solution C_2S–C_3P is precipitated from the liquid matrix slag. The CaO–SiO_2–FeO–P_2O_5 quaternary slag system is composed of P-rich phase, liquid matrix phase, and RO (metal oxides mainly formed by MgO and MnO) phase, and the P-rich phase mainly consists of solid solution C_2S–C_3P [33].

FESEM–EDS map scanning was further conducted to study the behavior of phosphorus enrichment in the slag phase. Fig. 7 shows the element distribution results of dephosphorization slag with the basicity of 2.59 by FESEM–EDS map scanning, and the corresponding FESEM picture is shown in Fig. 6(d). Table 5 shows the compositions of dephosphorization slag by FESEM–EDS point analyses in Fig. 7(a). By comparing the results of OM, XRD, and FESEM–EDS, we can find the highest contents of Si and P in the dark gray phase 1. The stoichiometric atom ratio of Si, P, and Ca in the solid solution C_2S–C_3P is 1:1:5, and the actual atom ratio of Si, P, and Ca in the dark gray phase 1 is approximately 3:2:8, which is close to that in the solid solution C_2S–C_3P. The dark gray phase 1 is the P-rich phase, which mainly contains solid solution C_2S–C_3P. The light gray phase 2 is continuously distributed in the dephosphorization slag (Figs. 6(a)–6(f)), which mainly contains Si, Mg, and Ca as well as a small amount of P, as shown in Fig. 7. Therefore,

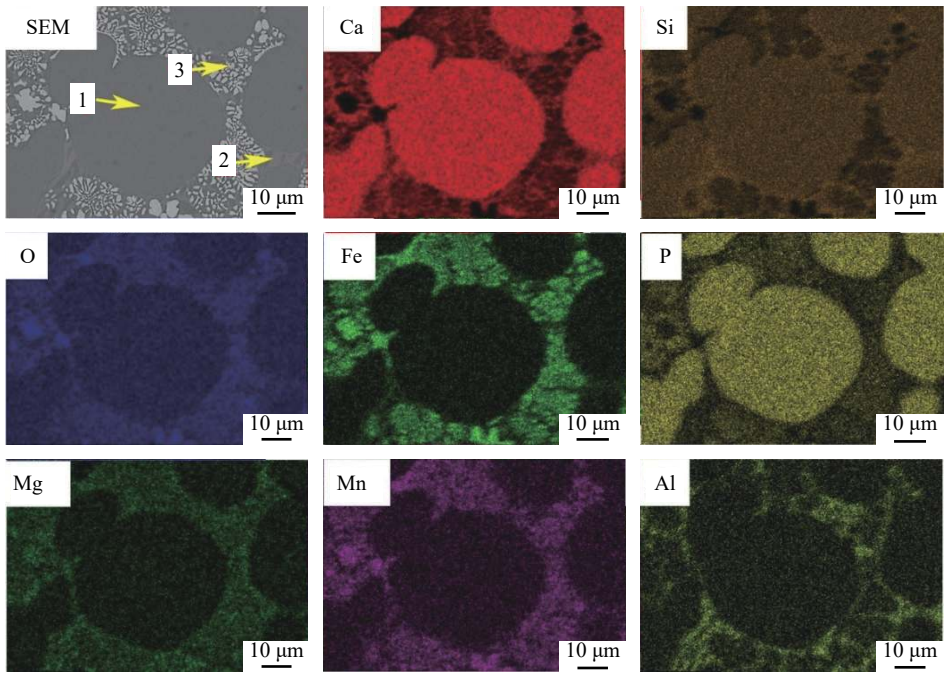

Fig. 7. Element distribution results of dephosphorization slag with the basicity of 2.59 by FESEM–EDS map scanning.

Table 5. Element compositions of dephosphorization slag by FESEM–EDS point analyses in Fig. 7(a)

Phase	O		Mg		Si		P		Ca		Mn		Fe		Al	
	wt%	at%	wt%	at%	wt%	at%	wt%	at%	wt%	at%	wt%	at%	wt%	at%	wt%	at%
1	37.01	57.52	0.74	0.77	10.55	9.37	7.01	5.62	38.84	24.15	3.14	1.42	2.59	1.15	0	0
2	31.65	55.49	1.85	2.16	7.14	7.15	2.68	2.43	21.29	14.93	9.89	5.04	23.47	11.76	0.59	0.61
2	23.35	47.95	5.45	7.46	1.46	1.71	0.67	0.71	5.65	4.64	17.75	10.60	46.64	26.58	0.18	0.21

the light gray phase 2 is the liquid slag phase, which is mainly composed of silicate $Ca_3Mg(SiO_4)_2$. On the other hand, the white phase 3 is closely distributed around the dark gray phase 1, which is substantially free of P and Si elements and has high contents of Fe, Mn, and Mg elements, and can be referred to as Fe-rich phase. In the white phase 3, the $Ca_2Fe_2O_5$ phase is formed. Thus, we can deduce that the CaO–FeO layer previously stated [25–28] is the $Ca_2Fe_2O_5$ phase, which can promote the formation of the solid solution C_2S–C_3P. A previous study showed that $3FeO{\cdot}P_2O_5$ can be formed in the slag, and then reacted with CaO to generate C_3P; then, the formed C_3P is combined with C_2S in the slag to generate solid solution C_2S–C_3P [34].

3.4. Effects of basicity on P-rich phase

Fig. 8 shows the calculated quaternary phase diagram for the slag of CaO–SiO_2–FeO–5wt%P_2O_5 at 1673 K by FactSage 7.3. The experimental data are marked in the same figure with the compositions from Table 3. The solid solution C_2S–C_3P can be precipitated in all the experimental slags. According to the calculation results in Fig. 8, in the slag with the high FeO content, the precipitation of solid solution C_2S–C_3P occurs, whereas in the slag with the high SiO_2 content, the solid solution C_2S–C_3P cannot be formed. Therefore, increasing the basicity of the slag is favorable to form the solid solution C_2S–C_3P.

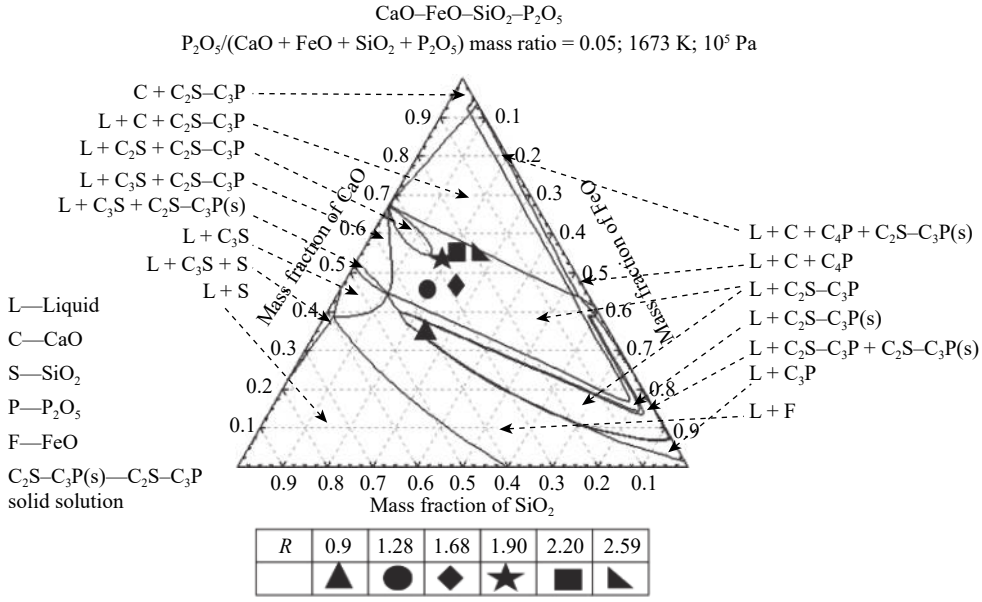

Fig. 8. Calculated quaternary phase diagram for slag of CaO–SiO_2–FeO–5wt%P_2O_5 at 1673 K.

Fig. 9 shows the FESEM images of dephosphorization slags at 1500 magnification with the different basicities whose compositions are shown in Table 3. Fig. 9(f) corresponds to Fig. 6 with the same slag sample. Table 6 shows the compositions of each slag phase with the different basicity. According to Fig. 9, the dephosphorization slags with basicities of 0.9 and 1.28 are made up of the dark gray P-rich phase and light gray liquid slag phase, but the white Fe-rich phase cannot be found, because forming a calcium ferrite phase under the condition of low basicity is difficult when the content of CaO is relatively low. De-P ratios at these two basicity values are relatively low as described in Table 2.

Figs. 9(c)–9(f) show phases 1, 2, and 3, which are the P-rich, liquid slag, and Fe-rich phases, respectively, and are consistent with the three phases described in Fig. 6.

With increasing basicity, the morphologies of the different phases in the dephosphorization slags change greatly. The P-rich phase changes from the thin strip shape at the basicities of 0.9–1.68 to the block shape at the basicities of 1.90–2.59. The liquid slag phase is the dendrite shape at the basicity of 0.9, and becomes the continuous network at the basicities of 1.28–2.59. The Fe-rich phase transforms from branch shape at the basicities of 1.68–2.20 to the block network at the basicity of 2.59.

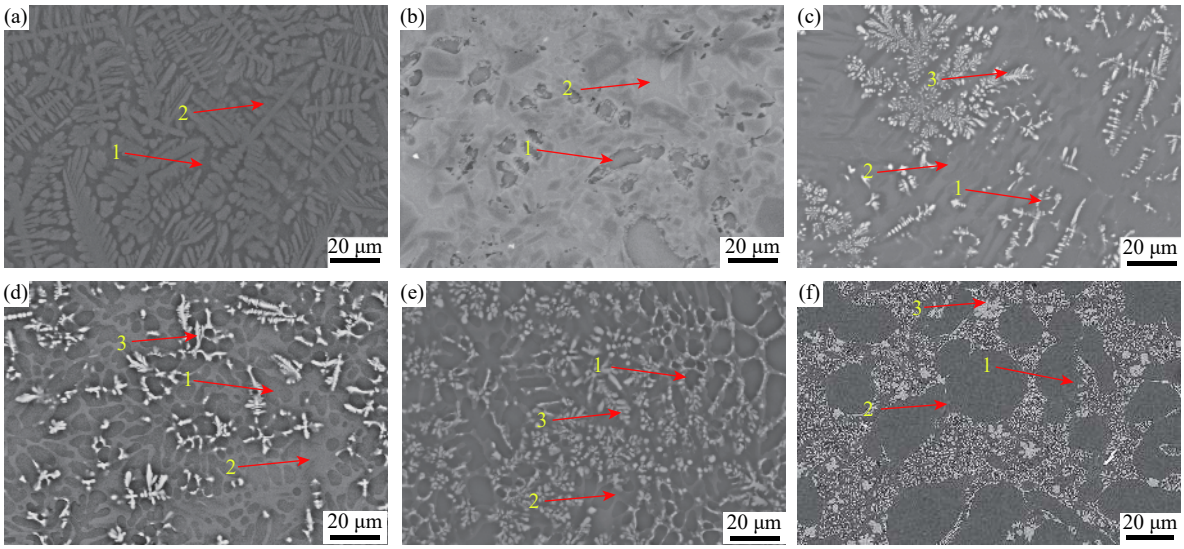

Fig. 9. FESEM images of dephosphorization slags with different *R* values: (a) 0.9; (b) 1.28; (c) 1.68; (d) 1.90; (e) 2.20; (f) 2.59.

Table 6. Composition of each phase in slags with different basicities (Fig. 9) wt%

R	Phase	SiO_2	P_2O_5	CaO	FeO	MnO	MgO	Al_2O_3
0.90	1	54.81	2.96	22.51	6.82	5.38	3.79	3.77
	2	49.35	2.68	22.48	8.51	7.51	8.60	1.18
1.28	1	40.43	11.74	37.91	3.48	3.35	2.24	0.07
	2	43.16	7.38	27.05	8.68	5.00	3.95	5.09
1.68	1	37.24	13.27	35.02	6.59	5.14	2.60	0.17
	2	43.95	8.45	29.10	8.23	5.16	4.12	1.53
	3	26.88	4.58	18.84	29.95	10.19	8.54	1.29
1.90	1	35.70	16.31	35.27	2.21	5.03	4.00	2.30
	2	39.06	5.64	25.95	4.01	6.97	6.11	12.11
	3	19.36	3.98	14.53	28.52	10.12	18.49	5.05
2.20	1	36.24	17.92	33.26	3.10	3.06	4.94	1.81
	2	27.45	6.53	37.96	4.90	4.72	8.57	9.53
	3	14.53	3.53	10.27	33.28	12.76	23.39	2.12
2.59	1	30.03	24.44	39.78	2.00	2.47	1.33	0
	2	26.31	11.15	27.46	21.62	8.26	3.98	1.69
	3	6.21	3.22	8.42	48.21	19.23	13.53	0.69

The area fraction of the P-rich and Fe-rich phases in Figs. 9(a)–9(f) is calculated by image analysis software. Fig. 10 shows the effects of dephosphorization slag basicity on the area fraction and P_2O_5 content of the P-rich phase. The area fraction and P_2O_5 content of the P-rich phase steadily increase as the basicity of the dephosphorization slag increases. This condition shows that increasing basicity can promote the formation of the P-rich phase containing the solid solution C_2S–C_3P, which is consistent with the results shown in Fig. 8. This is also the reason why increasing basicity can promote the De-P ratio, as shown in Fig. 3.

Fig. 11 indicates the effects of the area fraction of the Fe-rich phase on the P_2O_5 content and area fraction of the P-rich phase. When the basicities are 0.9 and 1.28, the area fractions of the Fe-rich phase are 0. When the basicity increases from 1.68 to 2.59, the area fraction of the Fe-rich phase changes from 23.12% to 42.27%, the area fraction of the P-rich phase rises from 15.35% to 49.65%, and the P_2O_5 content in the P-rich phase steadily increases from 13.27wt% to 24.44wt%. An obvious increasing tendency of the area fraction and P_2O_5 content of the P-rich phase occurs with increasing area fraction of the Fe-rich phase. This is because the phase ratio between the C_2S–C_3P solid solution and the total phases increases with increasing FeO content [28]. During the converter blowing process, the FeO content in the slag can be controlled by adjusting the oxygen lance position and oxygen supply flow rate, and increasing the amount and time of sinter. Thus, the area fraction of the Fe-rich phase in slag can be adjusted to promote the dephosphorization reaction.

From the preceding analysis of the different phases in the dephosphorization slag, we can deduce that the transfer route of P during dephosphorization is hot metal → liquid slag

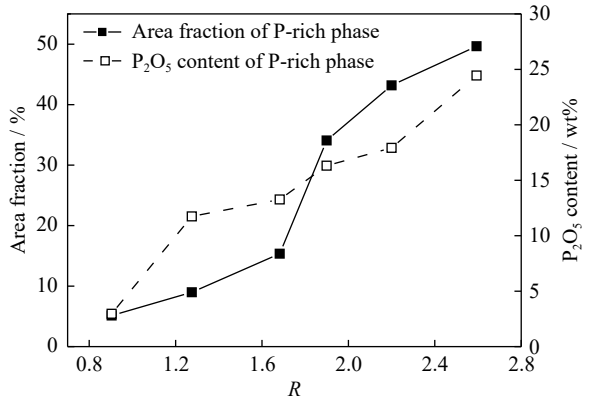

Fig. 10. Effects of slag basicity on area fraction and P_2O_5 content of P-rich phase.

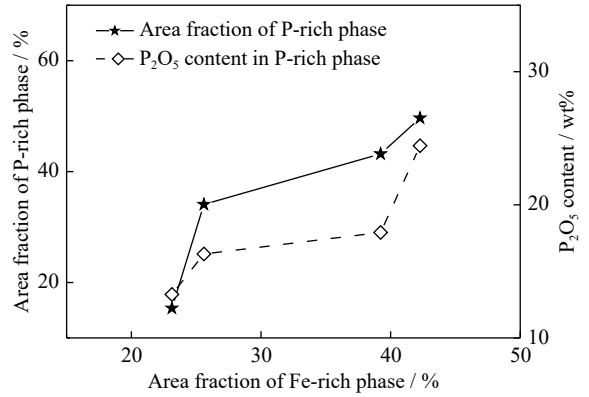

Fig. 11. Effects of area fraction of Fe-rich phase on area fraction and P_2O_5 content of P-rich phase.

phase + Fe-rich phase → P-rich phase. The reason is that as the area fraction of the Fe-rich phase increases, so do the area fraction and P_2O_5 content of the P-rich phase. Moreover, the P_2O_5 content in the P-rich phase ≧ that in the liquid slag phase ≧ that in the Fe-rich phase. When the P element enters the liquid slag phase and Fe-rich phase from the hot metal, it can be enriched around the dicalcium silicate (C_2S) to form the solid solution C_2S–C_3P in the P-rich phase, thereby promoting the dephosphorization reaction.

4. Conclusions

In this study, at low basicity and low temperature, the dephosphorization behavior and phosphorus distribution ratio L_P between slag and molten steel were studied through a 180 t BOF industrial experiment for the double slag and remaining slag process. The dephosphorization slags of different basicities were quantitatively analyzed. The conclusions are given as follows:

(1) At the low basicity range of 0.9–2.59, with increasing basicity of the dephosphorization slag, both L_P and dephosphorization ratio show an upward trend. The calculated L_P values by the empirical equations are reasonably higher than the experimental values.

(2) Dephosphorization slag is composed of the dark gray P-rich phase, light gray liquid slag phase, and white Fe-rich phase. The P-rich phase is mainly a solid solution of C_2S–C_3P. The liquid slag phase mostly consists of silicate and the Fe-rich phase primarily contains $Ca_2Fe_2O_5$.

(3) With increasing basicity, the morphologies of different phases in the dephosphorization slags are changed greatly, and the area fraction and P_2O_5 content of the P-rich phase are also increased. An obvious increasing tendency of the area fraction and P_2O_5 content of the P-rich phase occurs as the area fraction of the Fe-rich phase increases.

(4) The transfer route of P during dephosphorization can be deduced as hot metal → liquid slag phase + Fe-rich phase → P-rich phase. The reason is that as the area fraction of the Fe-rich phase increases, the area fraction and P_2O_5 content of the P-rich phase also increase. Moreover, the P_2O_5 content in the P-rich phase ≧ that in the liquid slag phase ≧ that in the Fe-rich phase.

Acknowledgement

This work was financially supported by the National Natural Science Foundation of China (No. U1960202).

References

[1] Y. Ogawa, M. Yano, S.-Y. Kitamura, and H. Hirata, Development of the continuous dephosphorization and decarburization process using BOF, *Steel Res. Int.*, 74(2003), No. 2, p. 70.

[2] N. Sasaki, Y. Ogawa, S. Mukawa, and K.-I. Miyamoto, Improvement in hot-metal dephosphorization, *Nippon Steel Tech. Rep.*, 104(2013), p. 26.

[3] M. Kobayashi, K. Isobe, and M. Arai, Technical progress in steelmaking and casting for special bar and wire steel at muroran works, *Nippon Steel Tech. Rep.*, 394(2012), p. 119.

[4] X.H. Wang, G.S. Zhu, H.B. Li, and Y.C. Lü, Investigation on "slag-remaining + double-slag" BOF steelmaking technology, *China Metall.*, 23(2013), No. 4, p. 40.

[5] X. Yang, F.M. Sun, J.L. Yang, F. Liu, K.S. Cheng, and J. H. Wang, Optimization of low phosphorus steel production with double slag process in BOF, *J. Iron Steel Res. Int.*, 20(2013), No. 8, p. 41.

[6] Z.H. Tian, B.H. Li, X.M. Zhang, and Z.H. Jiang, Double slag operation dephosphorization in BOF for producing low phosphorus steel, *J. Iron Steel Res. Int.*, 16(2009), No. 3, p. 6.

[7] J.F. Lü, Z.N. Jin, H.Y. Yang, L.L. Tong, G.B. Chen, and F.X. Xiao, Effect of the CaO/SiO2 mass ratio and FeO content on the viscosity of $CaO–SiO_2$–"FeO"–12wt%ZnO–3wt%Al_2O_3 slags, *Int. J. Miner. Metall. Mater.*, 24(2017), No. 7, p. 756.

[8] S. Kitamura, H. Shibata, K. Shimauchi, and S. Saito, The importance of dicalcium-silicate on hot metal dephosphorization reaction, *Revue De Métallurgie*, 105(2008), No. 5, p. 263.

[9] K. Ito, M. Yanagisawa, and N. Sano, Phosphorus distribution between solid $2CaO·SiO_2$ and molten $CaO–SiO_2–FeO–Fe_2O_3$ slags, *Tetsu-To-Hagané*, 68(1982), No. 2, p. 342.

[10] S. Kitamura, H. Shibata, and N. Maruoka, Kinetic model of hot

metal dephosphorization by liquid and solid coexisting slags, *Steel Res. Int.*, 79(2008), No. 8, p. 586.

[11] L. Lin, Y.P. Bao, M. Wang, H.M. Zhou, and L.Q. Zhang, Influence of SiO_2 modification on phosphorus enrichment in P bearing steelmaking slag, *Ironmaking Steelmaking*, 40(2013), No. 7, p. 521.

[12] J.Y. Li, M. Zhang, M. Guo, and X.M. Yang, Enrichment mechanism of phosphate in CaO–SiO_2–FeO–Fe_2O_3–P_2O_5 steelmaking slags, *Metall. Mater. Trans. B*, 45(2014), No. 5, p. 1666.

[13] X. Gao, H. Matsuura, and F. Tsukihashi, Phase equilibrium for the CaO–SiO_2–FeO–P_2O_5 system at 1673 K for dephosphorization with multi phase flux, *J. Iron Steel Res. Int.*, 18(2011), Suppl. 2, p. 84.

[14] X. Gao, H. Matsuura, I. Sohn, W.L. Wang, D.J. Min, and F. Tsukihashi, Phase relationship for the CaO–SiO_2–FeO–5 mass% P_2O_5 system with oxygen partial pressure of 10^{-8} atm at 1673 and 1623 K, *Mater. Trans.*, 54(2013), No. 4, p. 544.

[15] S. Kitamura, S. Saito, K. Utagawa, H. Shibata, and D.G.C. Robertson, Mass transfer of P_2O_5 between liquid slag and solid solution of 2CaO·SiO_2 and 3CaO·P_2O_5, *ISIJ Int.*, 49(2009), No. 12, p. 1838.

[16] S.L. Xie, W.L. Wang, Z.C. Luo, and D.Y. Huang, Mass transfer behavior of phosphorus from the liquid slag phase to solid 2CaO·SiO_2 in the multiphase dephosphorization slag, *Metall. Mater. Trans. B*, 47(2016), No. 3, p. 1583.

[17] R. Inoue and H. Suito, Phosphorous partition between 2CaO·SiO_2 particles and CaO–SiO_2–Fe_tO slags, *ISIJ Int.*, 46(2006), No. 2, p. 174.

[18] K. Shimauchi, S. Kitamura, and H. Shibata, Distribution of P_2O_5 between solid dicalcium silicate and liquid phases in CaO–SiO_2–Fe_2O_3 system, *ISIJ Int.*, 49(2009), No. 4, p. 505.

[19] X. Yang, H. Matsuura, and F. Tsukihashi, Reaction behavior of P_2O_5 at the interface between solid 2CaO·SiO_2 and liquid CaO–SiO_2–FeO_x–P_2O_5 slags saturated with solid 5CaO·SiO_2·P_2O_5 at 1573 K, *ISIJ Int.*, 50(2010), No. 5, p. 702.

[20] X. Yang, H. Matsuura, and F. Tsukihashi, Dissolution behavior of solid 5CaO·SiO_2·P_2O_5 in CaO–SiO_2–FeO_x slag, *Mater. Trans.*, 51(2010), No. 6, p. 1094.

[21] X. Yang, H. Matsuura, and F. Tsukihashi, Condensation of P_2O_5 at the interface between 2CaO·SiO_2 and CaO–SiO_2–FeO_x–P_2O_5 slag, *ISIJ Int.*, 49(2009), No. 9, p. 1298.

[22] C.M. Du, X. Gao, S. Ueda, and S. Kitamura, Distribution of P_2O_5 and Na_2O between solid solution and liquid phase in the CaO–SiO_2–Fe_2O_3–P_2O_5–Na_2O slag system with high P_2O_5 content, *Metall. Mater. Trans. B*, 49(2018), No. 1, p. 181.

[23] L. Lin, Y.P. Bao, C. Gu, W. Wu, and J.Q. Zeng, Distribution of P_2O_5 between P-rich phase and matrix phase in P-bearing steelmaking slag, *High Temp. Mater. Proc.*, 37(2018), No. 7, p. 655.

[24] F. Pahlevani, S. Kitamura, H. Shibata, and N. Maruoka, Distribution of P_2O_5 between solid solution of 2CaO·SiO_2–3CaO·P_2O_5 and liquid phase, *ISIJ Int.*, 50(2010), No. 6, p. 822.

[25] K. Ito and M. Terasawa, Utilization of multiphase fluxes for the dephosphorization of hot metal, *Steel Res. Int.*, 80(2009), No. 10, p. 733.

[26] T. Hamano, S. Fukagai, and F. Tsukihashi, Reaction mechanism between solid CaO and FeO_x–CaO–SiO_2–P_2O_5 slag at 1573 K, *ISIJ Int.*, 46(2006), No. 4, p. 490.

[27] X. Gao, H. Matsuura, I. Sohn, W.L Wang, D.J. Min, and F. Tsukihashi, Phase relationship of CaO–SiO_2–FeO–5 mass pct P_2O_5 system with low oxygen partial pressure at 1673 K (1400°C), *Metall. Mater. Trans. B*, 43(2012), No. 4, p. 694.

[28] S.L. Xie and W.L. Wang, Crystallization kinetics study of the (2CaO·SiO_2–3CaO·P_2O_5) solid solution in the multiphase dephosphorization flux, *Steel Res. Int.*, 87(2016), No. 3, p. 376.

[29] G.W. Healy, New look at phosphorus distribution, *J. Iron Steel Inst.* (*London*), 208(1970), No. 7, p. 664.

[30] H. Suito and R. Inoue, Phosphorus distribution between MgO-saturated CaO–Fe_tO–SiO_2–P_2O_5–MnO slags and liquid iron, *Trans. Iron Steel Inst. Jpn.*, 24(1984), No. 1, p. 40.

[31] K. Ide and R.J. Fruehan, Evaluation of phosphorus reaction equilibrium in steelmaking, *Iron Steelmaker*, 27(2000), No. 12, p. 65.

[32] X.F. Zhang, I.D. Sommerville, and J.M. Toguri, Equation for the equilibrium distribution of phosphorus between basic slags and steel, *Trans. Iron Steel Soc. AIME*, 6(1985), p. 29.

[33] H.M. Zhou, Y.P. Bao, and L. Lin, Effect of P_2O_5 on rich phosphorus phase of CaO–SiO_2–Fe_tO–P_2O_5 slag, *China Metall.*, 23(2013), No. 1, p. 45.

[34] S.L. Xie, W.L. Wang, D.Y. Huang, H.C. Li, and Y. Du, Clarification of the dissolution of solid CaO and the phosphorus-enrichment capability of calcium silicates in the multiphase slag based on the ion and molecule coexistence theory, *Steel Res. Int.*, 89(2018), No. 2, art. No. 1700317.